ACS OMEGA

Open Access

http://pubs.acs.org/journal/acsodf

Article

Influence of Various Flame Temperatures of the Gun Propellant on the Effectiveness of the Erosion Inhibitor and Relevant Mechanisms

Xijin Wang, Zhitao Liu,* Qian Chen, Jing Yang, Yao Zhu, You Fu, Yiming Ma, Feiyun Chen, and Xin Liao*

Cite This: *ACS Omega* 2024, 9, 9410−9423

Read Online

ACCESS | Metrics & More | Article Recommendations | Supporting Information

ABSTRACT: The development of high energy gun propellants faces significant challenges in terms of erosion, partly due to the inadequate effectiveness of erosion inhibitors. In this paper, the influence of quite different flame temperature of five gun-propellants on erosion-reducing efficiency of four representative inhibitors materials (talc/TiO_2/ PDMS/ Paraffin) were studied in vented erosion vessel tester. From aspects of morphologies and element compositions of erode steel samples, as well as the pressure and heat generated by propellant burning, the relevant erosion-reducing processes and mechanisms were discussed. The results indicated that erosion inhibitors should be appropriately selected according to the type of gun propellant. The erosion of gun propellants having extremely high flame temperature of 3810 K were hardly reduced using talc, TiO_2, and PDMS inhibitors, which can generate numerous solid particles aggravating the melt-wipe process. While paraffin exhibits a uniquely positive erosion-reducing efficiency for the gun propellant having a flame temperature of 3810 K, that was attributed to the mitigated melt-wipe process. The inference was further supported by the high-volume cooling gas, resulting from the higher burning pressure of propellants loading with paraffin and excellent heat absorption capacity of paraffin tested with propellants having higher propellant flame temperature. The obtained results indicated that the factors of flame temperature of gun propellants should be taken into the design and composition optimization of an effective inhibitor. This work could provide potential reference for the development of future novel inhibitors, which serves as high energy gun propellants.

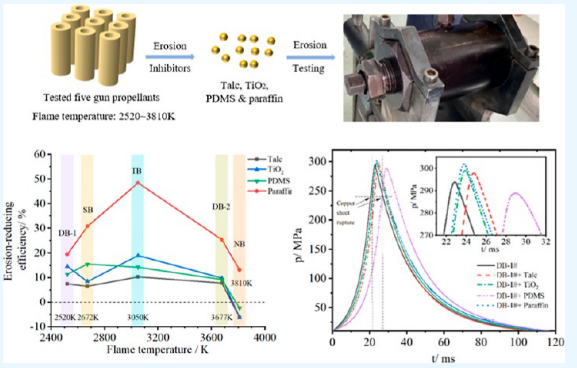

1. INTRODUCTION

High energy gun propellants containing balanced amounts of fuel and oxidants are required for modern high-chamber pressure gun weapons, which have enhanced muzzle velocity and range.[1−4] Compared with the conventional gun propellant, high energy gun propellants containing more powerful energetic materials, such as nitroglycerin (NG) and cyclotrimethylene trinitramine (RDX), have higher force constant and can produce higher flame temperature and higher volume gases in shooting process, which cause to enhanced erosion for gun barrel.[2−4] The severe erosion can result in the enlargement of the rifling origin or down bore area, thereby compromising ammunition performance and leading to reduced range and accuracy, fuze malfunctions, excessive muzzle flash, heightened torsional impulse, and blast overpressure, ultimately shortening the lifespan of the gun barrel.[1,5−7] It is generally recognized that mechanisms of erosion occurring both involves the thermal conduction, chemical reaction and mechanical wear between propellant gases and the gun steel surface.[6−10] Lawton gave a relation for gun wear that erosion mass varies exponentially with the maximum temperature of gun barrel and linearly with the chemical erosivity of the propellant.[6,8] The flame temperature of gun propellant and wear-reducing additives can significantly impact the heat transfer and maximum temperature of gun barrel during propellant firing.[6,8]

Up to now, the incorporation of wear-reducing additives into propellant charges has emerged as an efficient and low-cost technique, extensively employed in a diverse range of firearm systems over recent decades.[1,11−15] The inhibitors usually involve inorganic materials with a low thermal conductivity like talc, TiO_2 $CaCO_3$, and BN, and organic materials like paraffin and silicone.[1,8,11,12] These inhibitor materials can be directly incorporated into the gun propellant matrix[13,16,17] or added to the propellant charge placed between the projectile and propellant grains.[11,12,16] These inhibitors include not only single material like silicone oil, talc, TiO_2, K_2SO_4, and BN[1,6,8] but also the mixing of inorganic and

Received: November 6, 2023
Revised: January 24, 2024
Accepted: January 25, 2024
Published: February 12, 2024

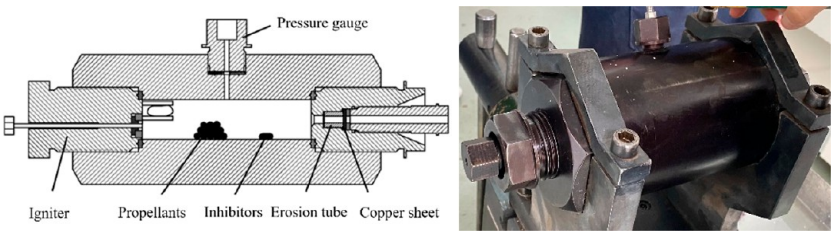

Figure 1. (Left) Diagram [Reprinted with permission from.[14] Copyright 2018 Wiley-VCH Verlag GmbH & Co. KGaA, Weinheim] and (right) photograph of the vented vessel erosion tester.

organic inhibitor materials like titanium dioxide (TiO_2)/paraffin, talc/paraffin, and microcapsules.[13−15] In this perspective, recent research efforts have been dedicated to the synthesis and optimization of composition for inhibitors.[14,15,21] Some types of inhibitors show significant erosion-reducing effects for general propellants, including single-, double-, triple-, and RDX-based gun propellants. However, conventional inhibitor materials also face challenges in achieving the desired erosion-reducing effect for propellants with higher energy due to the continuously increasing demand for modern high chamber pressure guns. These high energy propellants exhibit an enhanced flame temperature and severe erosion. The synthetic methodologies of inhibitors have been extensively studied in prior reports[14−21] which have also demonstrated their remarkable effectiveness in reducing erosion for a specific propellant formulation. However, the influence of flame temperatures on the inhibitor efficiency has rarely been extensively discussed in relation to various propellant composites. Moreover, the exact processes and mechanisms underlying erosion resistance in some inhibitor materials remain inadequately presented.

In this work, the influence of flame temperature of five gun-propellants on erosion-reducing efficiency of four representative inhibitors materials (talc/TiO_2/ PDMS/Paraffin) were studied. The five propellants have quite different flame temperature (2520−3810 K). Talc, TiO_2, PDMS and paraffin were four representative inhibitors materials, which usually serve as one component to manufacture many novel and effective composites inhibitor. Thus, we considered the four inhibitor materials to be appropriate references for the investigation of applicability between propellants and inhibitors. The erosion performance of propellants loading each inhibitor were first invested in vented erosion testing. Subsequently, from aspects of morphologies and element compositions of erode steel samples, as well as the pressure and heat generated by propellant burning, the relevant erosion resistance processes and mechanisms were discussed. This work aimed to provide a potential reference for designing future novel erosion inhibitors, which can achieve minimizing erosion for high energy gun propellants.

2. EXPERIMENT SECTION

2.1. Materials. Raw materials for manufacturing gun propellants are shown as follows: RDX (1−30 μm) and nitroguanidine (NQ, 5−30 μm) were purchased from Liaoning Qingyang Chemical Industry Group Co., Ltd., Liaoning, China. Nitrocellulose (NC), diphenylamine, and NC-NG propellant tablets, which are composed of 53.8 wt % NC (12.6 N %), 43.3 wt % NG, and 2.9 wt % centralite, were provided by Sichuan Nitrocell Co., China.

Inhibitor materials are presented as follows: Paraffin with a melting temperature of 52−54 °C was provided by Shanghai Sinopharm Chemical Reagent Co., Ltd., China. Paraffin was cut into small slices before erosion testing. TiO_2 (100 nm, anatase) was purchased from Aladdin Reagent Co., China. Polydimethylsiloxane (PDMS, 100 cps) was obtained from Usolf Co., China. Talc powder (8000 mesh) was provided by Shanghai Macklin Biochemical Co., Ltd., China.

2.2. Preparation and Properties of Gun Propellants. Five gun-propellants were labeled as DB-1#, SB#, TB#, DB-2#, and NB# samples, which had theoretical flame temperatures of 2520, 2672, 3050, 3677, and 3810 K and theoretical force constants of 956.2, 969.0, 1083.9, 1168.7, and 1243.7 kJ/kg, respectively. The properties were calculated by REAL software, which can calculate the thermophysical properties of propellants at high pressures and temperatures. The DB-1# and DB-2# samples belonged to double-based gun propellant, with the compositions referring to military standard.[22] The SB# and TB# samples belonged to single-based and triple-based gun propellants, referred to as the military standard.[23,24] NB# samples represented RDX-based propellants. DB-1# samples were commercial products provided by Sichuan Nitrocell Co., China. The DB-2#, SB#, TB# and NB# samples were laboratory-made products. The experimental parameters, compositions, and properties of propellant samples are shown in Tables S1 and S2 in Supporting Information.

The SB, TB, DB-2, and NB propellants were manufactured by a solvent extrusion technique. The preparation process was as follows: First, dried NC-NG propellant tablets or NC powders were mixed and plasticized by a mixture of acetone and ethanol (1:1 by volume) in a kneading machine for 2 h at 35 °C to form propellant dough. Second, RDX or NQ was added to a kneading machine, and the kneading continued for 2 h. After that, a homogeneous dough was obtained and placed in a single perforating mold. Through an extrusion molding process, a propellant strand was received. Then, the strand was cut into grains with a 4 cm length. Finally, all propellant grains were dried in air at 20 °C for 3 days and then dried in an oven at 50 °C for 5 days.

2.3. Measurements. *2.3.1. Erosion Testing.* The vented vessel erosion testing was employed to examine the erosion performances of propellants and the erosion-reducing effectiveness of inhibitors. The diagram and optical photo of the erosion tester are shown in Figure 1, which is a standard 100 cm^3 closed boom tester modified by placing a copper sheet and an erosion steel tube in it.[25] The erosion steel tube was manufactured from GB45# quality carbon structural steel.[26] In testing, the gases produced by propellant grains would break the copper sheet and then leak out from the erosion tube samples, resulting in a decrease in weight. The weight of the erosion tube was recorded before and after three successive

https://doi.org/10.1021/acsomega.3c08812
ACS Omega 2024, 9, 9410−9423

firings, and the weight loss was used to indicate the erosivity of the tested propellants. Additionally, to mitigate the impact of energy and pressure variables on erosion results, it is empirically possible to adjust the quantity of propellant charges tested so as to achieve a comparable maximum burning pressure within a range of 300 ± 10 MPa, which is determined by a pressure sensor plotting pressure−time curves. The experimental loading mass of propellant grains and inhibitor samples is listed in Table 1. The loading mass of each inhibitor was 3 wt % relative to that of the propellant charges in erosion testing and closed vessel testing. The inhibitors were placed between propellant grains and a erosion tube, as shown in Figure 1 (left); the silicone oil was injected into the position by an injector. The thickness of each copper sheet was 1.50 ± 0.02 mm, which would break experimentally at a pressure of ∼240 MPa.[27,28] All propellant grains were initiated by nichrome wire with igniting powder (NC, 11.88−12.40 N %, 1.000 g).

Table 1. Loading Mass of Tested Propellants and Inhibitors in Each Erosion Testing

loading mass	DB-1	SB	TB	DB-2	NB
propellants/g	25.8300	26.1975	24.0712	23.1000	21.4725
inhibitors/g	0.7749	0.7859	0.7221	0.6930	0.6442

2.3.2. Morphology and Element Composition for Eroded Steel. Scanning electron microscopy−energy-dispersive X-ray spectroscopy (SEM−EDX) analysis was employed to investigate the morphology and element composition of each erosion tube sample, which would be cut into two pieces along with the lengthways direction after three propellant firings. Each erosion tube was ultrasonically treated for 5 min in a mixture of ethanol and acetone (1:1) and dried. Following the inner surface of the erosion tube, samples were observed by SEM (QUANTA250FEG, FEIGECH) and an energy dispersive spectrometer. The observed position on the inner surface of the erosion tube was one end closer to the propellant charge, which was more severely eroded than the end away from the propellant charge. The method referred to the phenomenon that the more serious erosion would occur at the chamber throat than at the gun muzzle.

2.3.3. Closed Vessel Testing. The closed boom tester is a standard 100 cm^3 closed vessel tester (CV)[29] used to investigate the influence of inhibitors on the burning behaviors of propellant grains. The device diagram is shown in Figure S1 in Supporting Information. The testing was performed at a 0.2 g/cm^3 propellant loading density. All propellant grains were initiated by nichrome wire with the igniting powder (NC, 11.88−12.40 N %, 1.000 g), along with the pressure−times curves would be recorded by a pressure sensor.

2.3.4. Calorimeter Testing. The heat of explosion of the propellant and its combination with inhibitors was assessed using a Parr 6200 calorimeter. The tester diagram is shown in Figure S2 in Supporting Information. Each inhibitor sample was placed at the bottom of the crucible and weighed with 3 wt % of propellant grains. The tubular propellants grains were sliced into sheets with a diameter of approximately 1 mm, and each crucible contained 5.5 g of the sheets. The loading mass of each combination of propellant and inhibitor was 5.5 + 0.165 g. Then, the crucible was placed in the bomb calorimeter, which would be filled with 3.0 MPa nitrogen. Subsequently, the propellant samples were initiated by a nichrome wire and raised to the temperature of water in an adiabatic sleeve. Finally, according to the change in temperature of water, the heat of explosion of propellant could be calculated as follows

$$Q = \frac{m_w c_w \Delta T_w - Q_f}{m_p}$$

where Q (J/g) and Q_f (J/g) are the heat of explosion of propellant and heat released by the fuse, respectively; m_w (g) is the mass of water in each test; c_w (J/(g·°C)) is the heat capacity of water; ΔT_W is the temperature rising value of water; m_p (g) is the loading mass of propellant grains; Furthermore, the initial temperature of deionized water was 25 to 28 °C. The room temperature was 30 °C. For each propellant composition, two samples were tested.

3. RESULTS AND DISCUSSION

3.1. Erosion-Reducing Effect of Four Representative Inhibitors. The vented vessel erosion tester was employed to investigate the erosion performance (W) and erosion-reducing efficiency (E) of propellant charge loading with inhibitor materials. The W and E values were calculated by the following[14,15]

$$W = m_0 - m_1$$

$$E = (W_b - W_s)/W_b \times 100\%$$

where m_0 and m_1 are the weights of the erosion tube sample before and after three firings, respectively; W_b and W_s are the erosion performance values (W) of propellant charges without inhibitor and with inhibitor, respectively. Erosion of five propellants (DB-1#, SB#, TB#, DB-2#, and NB#) loading with four single inhibitor materials (talc, TiO_2, PDMS, and paraffin) were, respectively, tested, and the relevant W and E values were calculated.

As shown in Table 2, the five propellant samples (DB-1#, SB#, TB#, DB-2#, and NB#) loading without inhibitor exhibited a significant difference in W values of 0.91, 0.83, 1.48, 2.63, and 2.37 g. The difference is mainly derived from the temperature and chemical erosivity of propellant gas products. According to Lawton's correlation[6]

Table 2. Erosion Performance (W) of Propellant Loading with Inhibitor Materials

	erosion performance value (W)/g				
propellants	none inhibitor	talc	TiO_2	PDMS	paraffin
DB-1#	0.91	0.84	0.78	0.81	0.73
SB#	0.83	0.78	0.76	0.70	0.58
TB#	1.48	1.22	1.2	1.27	0.76
DB-2#	2.63	2.43	2.38	2.39	1.96
NB#	2.37	2.52	2.52	2.44	2.06

$$W = Ae^{BT_{max}}$$

the chemical erosivity of gases influences wear through the coefficient A, and the erosive wear (W) is approximated by an exponential function of maximum bore temperature (T_{max}), suggesting that bore temperature has a significant impact on erosion occurrence. After incorporating inhibitor materials into propellant charge, the W values of DB-1#, SB#, TB#, and DB-2# show both reduction tendencies. While the W values of

https://doi.org/10.1021/acsomega.3c08812
ACS Omega 2024, 9, 9410−9423

NB# propellant loading with Talc, TiO_2, and PDMS are not reduced.

As shown in Figure 2, the E values more clearly presented the erosion-reducing effect of a single inhibitor for propellants

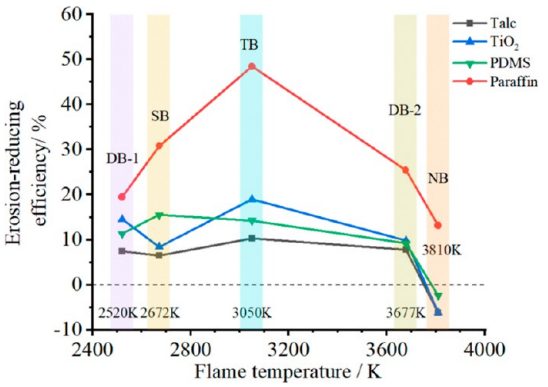

Figure 2. Erosion-reducing efficiency (E) of propellant loading with inhibitor materials.

with different flame temperatures, as well as the detailed E values shown in Table S3 in Supporting Information. Paraffin exhibited significant erosion resistance for all five propellant compositions, with E values of 19.78, 30.12, 48.65, 25.48, and 13.08% corresponding to flame temperature values of 2520, 2672, 3050, 3677, and 3810 K. Meanwhile, Talc, TiO_2, and PDMS show similar E values ranging from 6.02 to 18.92% within the flame temperature range of 2520−3677 K. While the three inhibitor materials, respectively, exhibited E values of −6.33, −6.33, and −2.95% at a flame temperature of 3810 K, this resulted from NB# propellant, a phenomenon that has rarely been reported. We subsequently attempted to explain it based on the more experiments performed in variable inhibitor material conditions and detailed characterization in aspects such as morphologies of eroded steel, pressure generated by propellant, and heat capacity of inhibitors at high temperatures.

3.2. Erosion Appearance, Chemical Composition, and Morphology of the Steel Interface. To further investigate the erosion resistance process of four representative inhibitor materials under different flame temperature conditions, the erosion tube samples were cut along the lengthwise direction to expose the inner surface of eroded steel after three propellant firings. All steel samples underwent through ultrasonic cleaning in alcohol/acetone and removal of impurities before comprehensive characterizations in this work. The following SEM−EDX mapping analysis was performed on the morphologies and chemical compositions of the sample's surface.

3.2.1. Erosion Appearance. Figure 3 exhibits the erosion appearance of steel samples after firing propellant loading without an inhibitor. The inner diameters of erosion tube samples were clearly increased after firing propellants, along with the mass reduction. The color of the erosion tube samples significantly varied after firing. All the above features suggest that erosion is occurring. Moreover, the appearance colors of DB-2# and NB# turned black (Figure 3e,f), indicating more severe erosion, which agrees with the erosion testing results values in the above section.

Figure 4 shows the appearance of erosion tube steel samples after firing DB-1# and NB# propellants loaded with the single inhibitors of Talc, TiO_2, PDMS, and paraffin. Additional

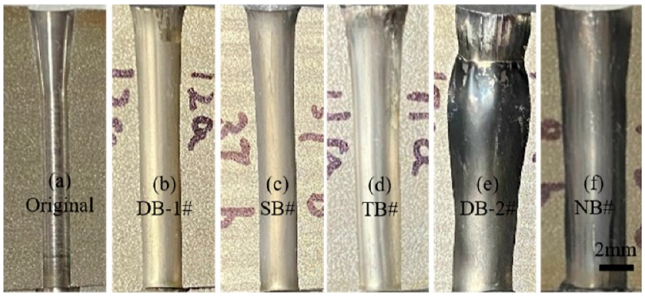

Figure 3. Photograph of steel samples fired by propellant loading without the inhibitor.

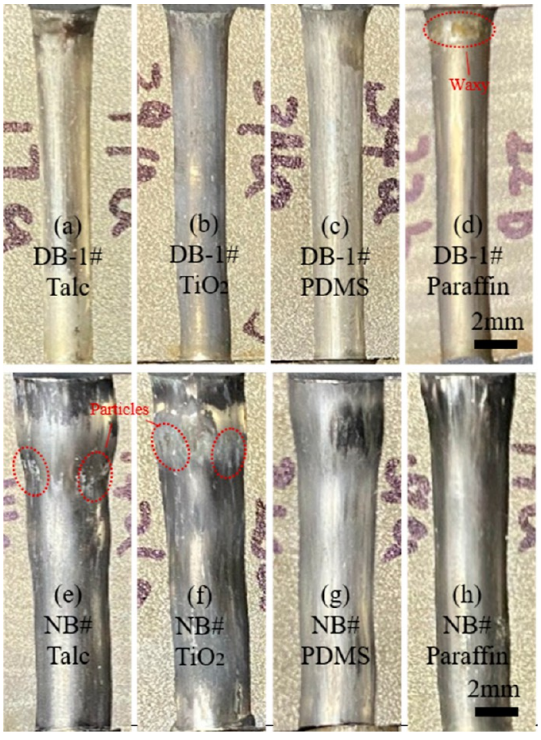

Figure 4. Photograph of steel samples fired propellants loading with talc, TiO_2, PDMS, and paraffin.

images of steel samples fired by SB#, TB#, and DB-2# propellants are shown in Figure S3 in Supporting Information. Compared with the firing of DB-1# and NB# propellants without the inhibitor, as shown in Figure 4, the incorporation of Talc and TiO_2 inhibitors exhibited the obvious coverage of white particles on the steel interface. The introduction of PDMS and paraffin loading resulted in the steel interface slightly turning white and bright for NB# propellant. Moreover, it is notable that the presence of a waxy substance was observed on the steel interface of DB-1#/paraffin, as shown in Figure 4e. The phenomenon was probably attributed to the fact that the paraffin loadings are hardly fully decomposed in the firing of DB-1# propellant, which has a relative low flame temperature and insufficient heat conditions.

3.2.2. Chemical Composition. To exactly determine the chemical variation on the surface of steel samples, which were investigated by SEM−EDX mapping analysis. Figure 5 exhibits the results of the chemical composition of the steel interface fired by propellant loading without the inhibitor. The EDX chemical element distribution mappings are presented in Figures S4−S17 in Supporting Information. The enrichment of

https://doi.org/10.1021/acsomega.3c08812
ACS Omega 2024, 9, 9410−9423

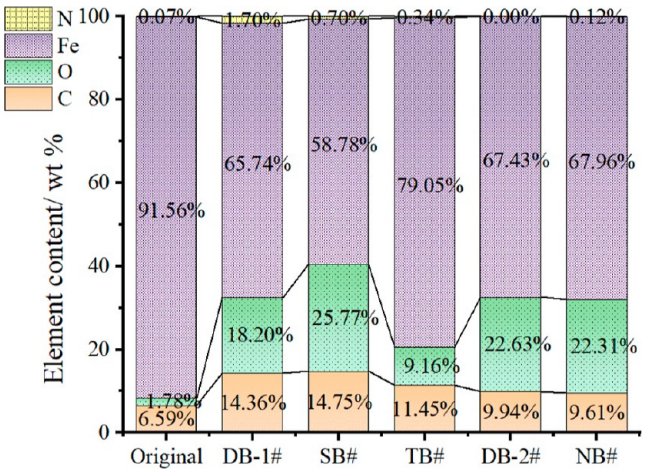

Figure 5. Element content of the steel surface fired by the propellant.

elements on mapping further provided support for observed substances, which can be identified as inhibitor products on steel.

As shown in Figure 5, the chemical composition of the original erosion tube steel interface contained carbon ©, oxygen (O), ferrum (Fe), and nitrogen (N) elements, with mass percents of 6.59, 1.78, 91.56, and 0.07%, respectively. After propellant combustion, there was an observed increase in the concentration of C and O elements within the steel samples of all five propellant charges. It was suggested that additional C and O elements originated from the propellant compositions. The C content exhibited a significant decrease as propellant flame temperature increased, with the C content reducing from 14.36 to 9.61% for DB-1#−NB# propellants. This phenomenon could be attributed to the following reasons: First, the combustion of carbon-containing propellant generates CO and CO_2. High percent CO provides monatomic C at the hot gas−steel interface by reactions[30−32]

$$CO \leftrightarrow C + O$$

$$CO_2 + C \leftrightarrow 2CO$$

Subsequently, the resulting C element subsequently diffuses into the gun steel, forming a solid solution, and precipitates as iron cementite (Fe_3C) through reactions[30,32]

$$3Fe + 2CO = Fe_3C + CO_2$$

In this work, as shown in Table 3, the gas product compositions of DB-1# and SB# propellants contain more CO and less CO_2 among all five propellant samples, which can result in a high content of Fe_3C generated in the gas−steel interface based on the above theory. As the propellant flame temperature increases, the decrease in CO content and the increase in CO_2 content lead to the decreasing tendency of the C element in the steel interface fired by DB-2# and NB#. Additionally, the O content of the TB# steel sample was lower than that of other samples, measuring at 9.16%. This could be attributed to a higher percentage of N_2 in the gas product composition of TB# propellant, which relates to the protective effects of nitrogen,[32] effectively reducing the chemical erosivity of gases at the steel interface.[33,34]

Table 3. Theoretical Composition of Propellant Gas Products by REAL Software

	propellant gases composition (mole percentage)				
propellants	H_2/%	CO/%	CO_2/%	H_2O/%	N_2/%
DB-1#	21.41	50.27	4.63	13.47	10.22
SB#	11.28	44.24	10.86	22.38	11.25
TB#	12.31	27.48	7	25.18	28.04
DB-2#	6.22	34.29	17.1	28.15	14.24
NB#	6.89	31.42	13.28	26.85	21.57

Figures 6 and 7 present the chemical composition of the eroded steel interface after the introduction of four

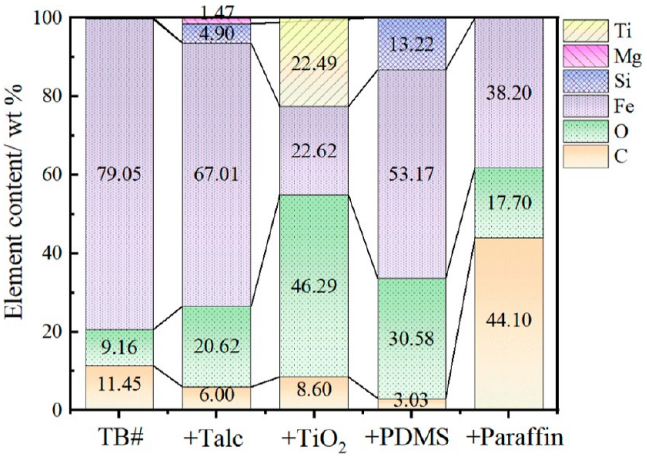

Figure 6. Element composition of steel samples fired by the TB# propellant with talc, TiO_2, PDMS, and paraffin.

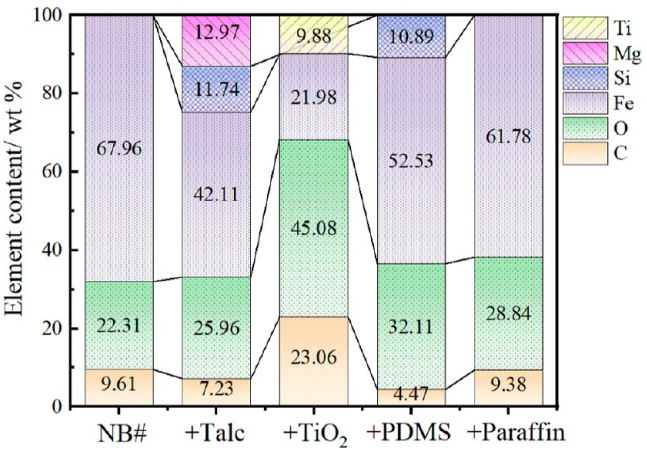

Figure 7. Element composition of steel samples fired by the NB# propellant with talc, TiO_2, PDMS, and paraffin.

representative inhibitors in the firing of TB# and NB# propellants. It is clear that O element contents on the steel interface were increased for both TB# and NB# propellants, adding four representative inhibitors. The incorporation of talc resulted in the introduction of silicon (Si) and magnesium (Mg) elements on the steel interface, with Si and Mg values of 4.9 and 1.47%, respectively, after the firing of the TB#/talc combination and Si and Mg values of 11.74 and 12.97%, respectively, after the firing of the NB# talc combination. The incorporation of TiO_2 introduced titanium (Ti) elements on a steel interface, with Ti values of 22.49 and 9.88% for the firing of TB#/TiO_2 and NB#/TiO_2 combinations. The PDMS loadings introduced Si elements on the steel interface, with Si values of 13.22 and 10.89% for the firing of TB#/PDMS and

https://doi.org/10.1021/acsomega.3c08812
ACS Omega 2024, 9, 9410−9423

NB#/PDMS combinations. The paraffin loading resulted in an increased C element content on the steel interface after firing the TB#/Paraffin combination. The introduction of additional elements is due to the oxidation and decomposition products of four inhibitors at high temperatures, forming relevant oxide substance layers on steel interfaces. The phenomena agree with the presumption of relevant wear-reducing additive mechanisms that the protective layer depositing on bore results in a reduction in heat transfer and temperature on bore surface in the previous study.[8]

3.2.3. Surface Morphology of Steel Samples. To further study the mechanisms attributing suitability matching relationship between flame temperature factors and inhibitor materials, the detailed morphology characterization of eroded steel interfaces was observed by SEM at variable magnification.

3.2.3.1. Without Inhibitor. Figures 8 and 9 present the SEM image of the interface of the uneroded steel sample and the

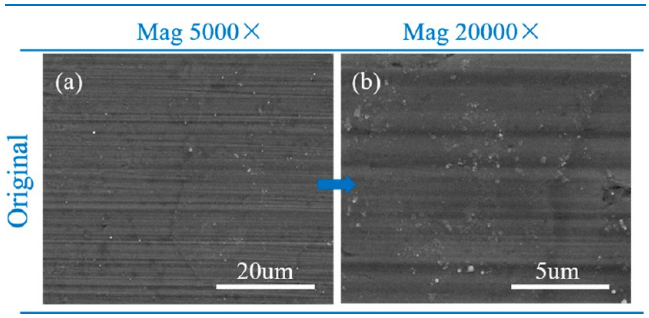

Figure 8. SEM images of the uneroded steel sample: (a) Mag 5000× and (b) Mag 20 000 ×.

eroded steel sample after firing five propellants without the inhibitor. As shown in Figure 8a,b, the uneroded steel sample exhibited a smooth surface appearance. After propellant firing, as shown in Figure 9a−d, the steel interfaces eroded by DB-1# and SB# propellants exhibited a rough appearance with few cracks. The DB-1# and SB# propellants, having a relatively low flame temperature, caused the absence of melting. The erosion may have occurred by the mechanical action of propellant gases flowing on a thermally softened steel surface.[6,32] In contrast, as shown in Figure 9e−j, TB#, DB-2#, and NB# propellants resulted in more cracks on the steel surface. The formation of cracks derives from stress generated in a steep temperature gradient[32] and disparate volumes of various iron phases generated in the heat-affected zone.[35] In addition, severe melting was observed on the steel surface fired by DB-2 #and NB# propellants. The melting phenomenon was consistent with the so-called melt-wipe process.[32] The surface steel is melted at high temperatures, and the liquid iron is wiped away through the mechanical action of solid propellant particles within the propellant gas product flow.[32] The obvious melting and cracks enable thermal and chemical to be dominant factors for erosion, indicating that five propellants can cause quite different temperatures on the steel surface and suggesting various dominant erosion mechanisms. Meanwhile, this can possibly lead to variable erosion-reducing effects of one inhibitor when different propellants are fired due to the different heating effects.

3.2.3.2. Talc. The appearance of raw talc was sheets-structured particles with a size of 1−10 μm, as shown in Figure S18 in Supporting Information. Figure 10 shows the morphologies of the steel surface eroded by five propellants

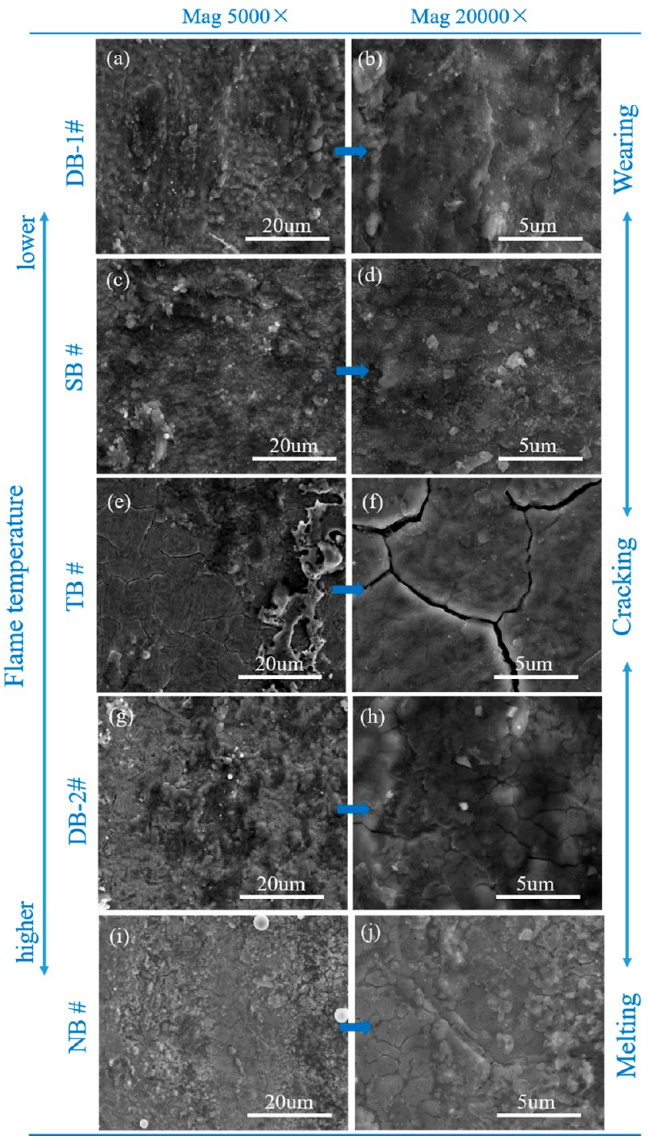

Figure 9. SEM images of (a,b) DB-1#, (c,d) SB#, (e,f)TB#, (g,h)DB-2#, and (i,j)NB# steel sample.

loaded with Talc particles. It is notable that there are many particles left on the steel surface that exhibit various morphologies in different propellant firings, which were identified to contain Si, Mg, and O elements in the above EDX analysis. As shown in Figure 10a−d, talc particles were dispersed on a steel surface with a sheet-like appearance like raw talc. As for the TB# propellant, as shown in Figure 10c,f, the talc particles were reconstructed into a flat protective layer structure on the steel surface. The partial delamination of the surface layer may have been caused by ultrasonic cleaning prior to observation. In the case of DB-2 and NB propellants, as shown in Figure 10g−i, talc exhibited a severe agglomerated appearance and was unabled to disperse well in the steel interface. The agglomerated structures of talc particles were significantly different compared to the appearance of DB-1#, SB#, and TB# steel samples. The various morphologies of talc products are attributed to the following reasons:

Previous reports propose the decomposition of talc involving various types of dehydration and formation processes for products, including enstatite, silica, quartz, and other amorphous species.[36−39] The dehydration of talc begins at

https://doi.org/10.1021/acsomega.3c08812
ACS Omega 2024, 9, 9410−9423

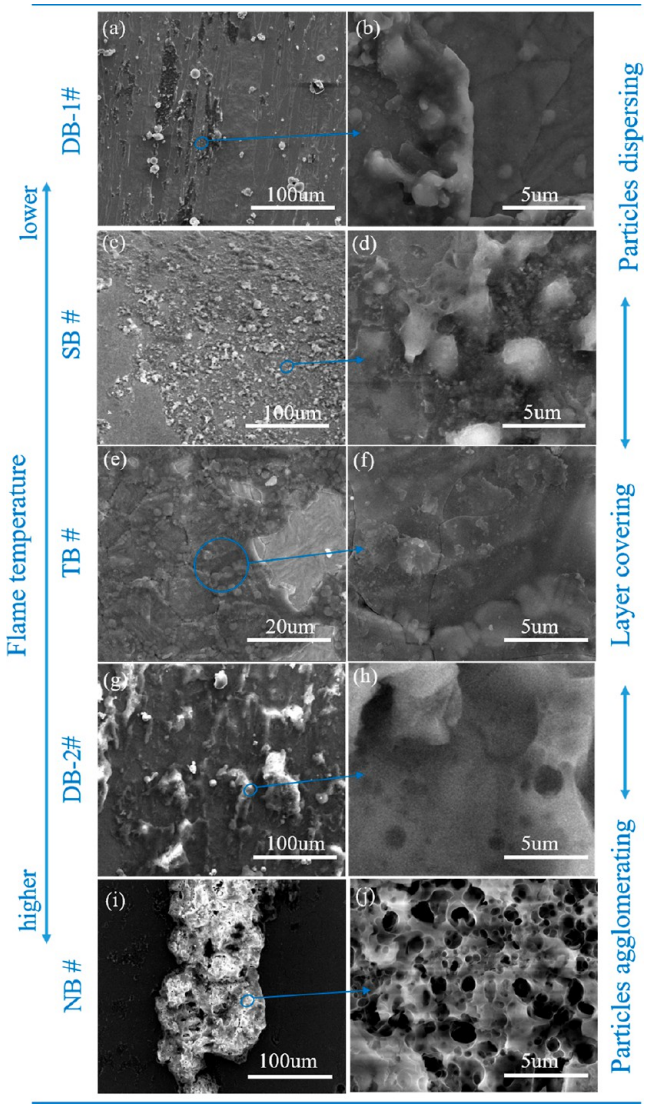

Figure 10. SEM images of (a,b)DB-1#, (c,d)SB#, (e,f)TB#, (g,h)DB-2#, and (e,f)NB# steel sample loading with talc particles.

800 °C and dehydroxylates completely after 1000 °C,[36] with the formation of enstatite only at 800 °C and the formation of enstatite, silica, and quartz at 800−1000 °C.[37] And the enstatite changes gradually to protoenstatite at ∼1200 °C, along with the amorphous silica converted to cristobalite at ∼1300 °C.[38] Talc decomposes in a single step to form $MgSiO_3$ and cristoblite at 1473−1600 °C.[39] It is suggested that different heating temperatures result in different talc-decomposed products.

In this work, talc as an inhibitor of hydrous minerals was heated by the combustion of five propellant samples at different flame temperatures, thereby converting into variable products. The formation process is confirmed by heterogeneous nucleation, growth, and recrystallization mechanism.[37] This is responsible for the various morphologies of talc products on the steel surface in different propellant erosion tests. In the case of DB-1# and SB# propellant, low bore temperatures are insufficient to completely decompose talc. In the case of DB#-2 and NB# propellants, high bore temperatures caused the talc to dehydroxylate completely and recrystallize, resulting in the agglomeration products on the steel interface after firing of DB-2#/talc and NB#/talc combinations. The agglomeration of talc products not only resulted in larger agglomerated particles and the absence of a protective layer covering the steel but also possibly aggravated the melt-wipe process occurring on the melting steel interface during NB# propellant firing. This eventually led to the ineffectiveness of talc against the NB# propellant and increased erosion. Moreover, this suggestion can be supported by Song's theory in previous work.[20] In his work, nanoparticle inhibitors with poor dispersion in the propellant matrix can result in numerous large particles, which leads to increased wear in the gun bore. In contrast, the agglomerated large particles derived from increased flame temperature should be the main case of aggravated NB# propellant erosion in this paper.

3.2.3.3. TiO_2. Figure 11 shows the morphologies of the steel surface eroded by DB-1#, TB#, DB-2#, and NB# propellants

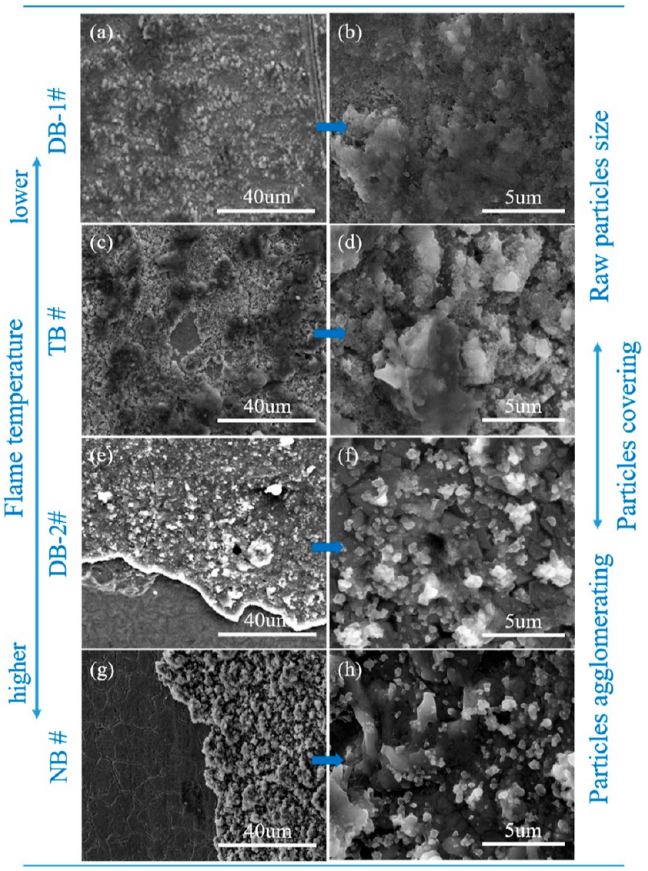

Figure 11. SEM images of (a,b)DB-1#, (c,d) TB#, (e,f)DB-2#, and (g,h)NB# steel sample loading with TiO_2 particles.

loaded with TiO_2 particles. As shown in Figure 11a−d, TiO_2 resulted in the formation of a densely particles-protective layer on the steel surface after DB-1#/Talc and TB#/Talc combinations firing, along with the particles layer containing Ti, O, and C elements in the above EDX results. It is notable that TiO_2 particles are well-dispersed on the steel interface fired by DB-1# propellants, compared to talc. This corresponded to the erosion testing results showing that the DB-1#/TiO_2 combination showed less erosion than the DB-1#/talc combination. This should be attributed to the smaller particle size of TiO_2 (∼100 nm) than talc (∼10 μm) in this work, as the appearance of raw TiO_2 shown in Figure S18 in Supporting Information. The particle size should influence the effectiveness of inhibitors.[16]

https://doi.org/10.1021/acsomega.3c08812
ACS Omega 2024, 9, 9410−9423

As shown in Figures 11a–d and S18d–f, after DB-1#/TiO_2 and TB#/TiO_2 propellant firing, the particle size of the TiO_2 protective layer was close to the raw TiO_2 particle size. As shown in Figure 11e–h, after DB-2# and NB# combination specimen firing, the TiO_2 particles within the protective layer exhibited agglomeration, along with the obviously increased particle size, due to the propellant flame temperature increasing. The TiO_2-transferred crystal structure can account for the phenomenon. According to previous reports, TiO_2 undergoes anatase transformations to the rutile phase at 620–802 °C,[40−42] with the rutile phase being well thermostable and having a melting temperature of 1830 °C.[43] The small TiO_2 particles have a tendency to spontaneously agglomerate into big particles along with the phase transformation process at elevated temperatures.[44] In this work, the high fame temperature of DB-2# and NB# propellants resulted in the agglomeration of TiO_2 particles and the reduced coverage effect of the protective particle layer. In the combustion process of NB#/TiO_2 combination specimens, these particles should be within the flow of propellant gases, possibly striking the melting gas–steel interface and aggravating the melt-wipe process, similar to the action of the NB#/Talc case.

3.2.3.4. PDMS. Silicone oil is a typical liquid artillery erosion inhibitor and is usually carried in a bag and placed in the cartridge with propellant grains behind the projectile. Meanwhile, polydimethylsiloxane (PDMS) is a useful inhibitory liquid among silicone oil substances.[14] Therefore, the erosion-reducing efficiency of PDMS was investigated under different propellant flame temperature conditions in this work. To enhance the contact area and achieve the greatest possible corrosion inhibition, PDMS was directly injected by the injector and coated onto the propellant surface.

As shown in Figure 12, PDMS led to a lot of particle-like and layer-like residues on the erosion tube steel surface, which have been identified by EDX mapping analysis (Figures 6 and 7) as silica oxide products. In the case of DB-1#, SB#, TB#, and DB-2# steel samples, as shown in Figure 12a–h, the PDMS products had a layer appearance. These layers could provide the protective action for the steel interface from hot gas, derived from reduced heat transfer based on relevant previous theory and erosion testing results in Figure 2. However, after NB#/PDMS combination firing, as shown in Figure 12i,j, the PDMS products on the steel interface tended to show an agglomerated particle appearance and achieved low coverage at the steel interface. The corresponding erosion testing results in Figure 2 exhibit that the NB#/PDMS combination has decreased erosion compared to the NB#/Talc and NB#/TiO_2 combinations but still shows enhanced erosion compared to the noninhibitor NB# propellant. Therefore, the observed PDMS particle-like products could still be possibly responsible for the increased erosion in melting steel surfaces when firing NB# propellant with a flame temperature above 3810 K due to the presence of the melt-wipe process.

3.2.3.5. Paraffin. In this work, paraffin was the sole organic inhibitor, theoretically generating a nonsolid product at high temperatures due to its fully hydrocarbon composition. As shown in Figure 13, steel surfaces after paraffin introduction were notable clean and exhibited no particle residues and fewer cracks compared to steel surfaces after corresponding propellants fired without inhibitors and with the other three inhibitors. Meanwhile, each propellant/paraffin combination firing showed minimal erosion performance in all tested propellant combination firings. The phenomenon suggested

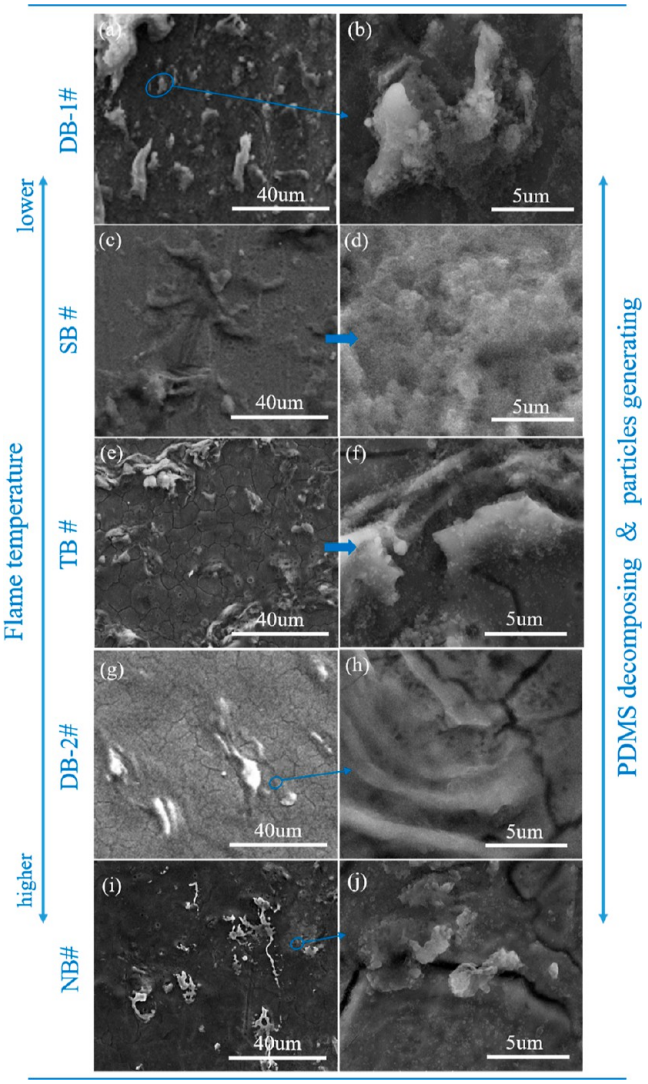

Figure 12. SEM images of (a,b)DB-1#, (c,d)SB#, (e,f)TB#, (g,h)DB-2#, and (i,j)NB# steel samples loading with PDMS.

that paraffin was heated into a gaseous vapor state and could reduce propellant erosion significantly. This could conclude that the antierosion mechanism of paraffin was different from the other three antierosion additives, which can form a particle-protective layer on steel surfaces. Moreover, in view of the unique positive erosion-reducing efficiency (13.18%) of the NB#/paraffin combination in all firings of NB# propellant loading with inhibitors, as shown in Figure 2 and Table S3, clean propellant gas flow without particles should be beneficial to the reduction in melt-wipe process presenting in propellant high flame temperature conditions and thereby mitigate erosion.

3.3. Burning Pressure Testing. In this work, to offset the influence of energy and combustion pressure on erosion results due to the various propellant composites, the loading mass of each propellant sample was set according to the empirically preestimated pressure generated of ∼300 MPa, which aimed to simulate the chamber pressure of the typical artillery. Tables 1 and 4 show the loading mass and the recorded maximum burning pressure (p_m) of each tested propellant in the vented vessel erosion tester, respectively. The pressure–time (p–t) curves of the whole erosion processes of each propellant

https://doi.org/10.1021/acsomega.3c08812
ACS Omega 2024, 9, 9410−9423

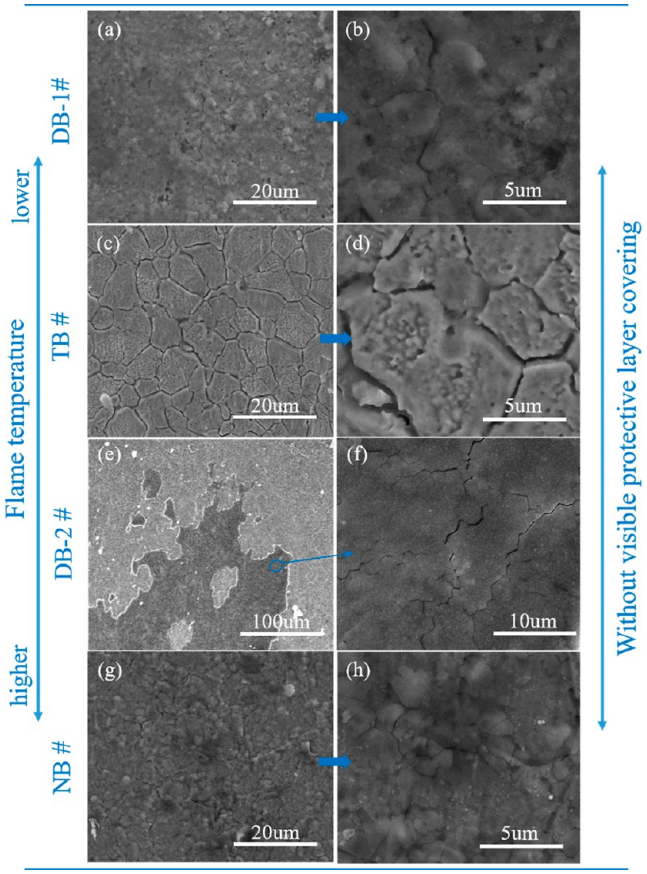

Figure 13. SEM images of (a,b)DB-1#, (c,d)TB#, (e,f)DB-2#, and (g,h) NB# steel sample loading with paraffin.

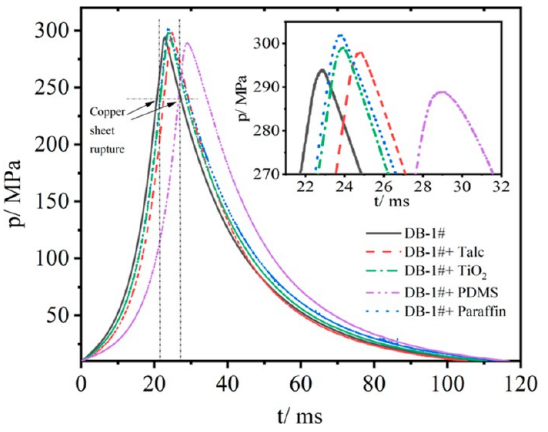

Figure 14. Pressure−time curves of DB-1# propellant loading with inhibitor during the erosion process in a vented vessel erosion tester.

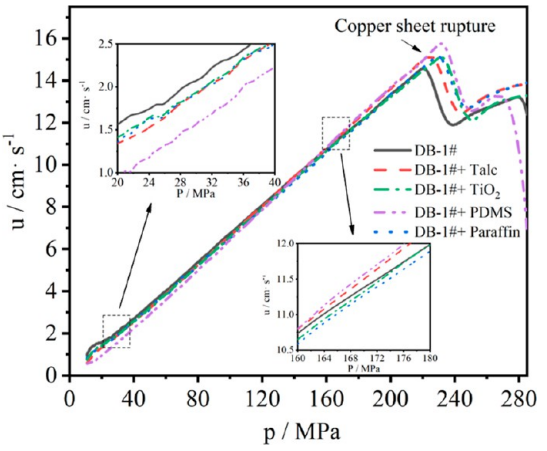

Figure 15. Burning rate−pressure (u−p) curves of DB-1# propellant loading with the inhibitor in the vented vessel erosion tester.

loading with inhibitors are presented in Figures 14 and S19, S20, in which the points of copper sheet rupture are marked according to the pressure values corresponding to decreased burning rate in Figures 15 and S21, 22.

As shown in Table 4, the p_m of DB-1#, SB#, TB#, DB-2#, and NB# propellants is 293.9, 304.9, 307, 311.8, and 310.9 MPa, respectively. All propellant charges can be regarded as generating erosion in similar pressure conditions. After inhibitors were incorporated into propellant charges, three solid inhibitors of talc, TiO_2, and paraffin resulted in increased burning pressure in erosion testing, with the mean value of p_m increasing by 3.1, 3.3, and 6.3 MPa. While PDMS resulted in decreased burning pressure, with the mean value of p_m decreasing by 3.0 MPa.

The phenomenon could be accounted for by the following reasons: First, despite the fact that inhibitors are nonenergetic materials, it still lead to an increase in propellant loading density in a constant volume vessel, and thus, the pressure slightly increased after talc and TiO_2 were introduced. Subsequently, the higher burning pressure after paraffin incorporation should be attributed to the high volume of paraffin vapor at high temperatures due to its formula ($C_{20\sim}H_{40\sim}$) containing more carbon and hydrogen. This effect should facilitate the dilution of propellant gases contacting the steel interface.

On the other hand, the decreased p_m caused by PDMS in Figure 14 should be due to the prolonged burning time and vented gas time. Figure 15 provides the burning rate−pressure

Table 4. Maximum Burning Pressure (p_m) of Propellants Loading with Inhibitors in a Vented Vessel Erosion Tester[a]

	none/MPa		talc/MPa		TiO_2/MPa		PDMS/MPa		paraffin/MPa	
propellants	p_m	Δp	p_m	Δp	p_m	Δp	p_m	Δp	p_m	Δp
DB-1#	293.9		298.0	4.1	299.1	5.2	288.9	−5.0	301.9	8.0
SB#	304.9		308.3	3.4	310.0	5.1	304.1	−0.8	313.0	8.1
TB#	307.0		310.4	3.4	308.8	1.8	299.7	−7.3	311.5	4.5
DB-2#	311.8		315.8	4.0	314.9	3.1	315.0	3.2	311.7	−0.1
NB#	310.9		311.4	0.5	312.3	1.4	306.0	−4.9	321.7	10.8
Mean value	305.7		308.8	3.1	309.0	3.3	302.7	−3.0	312.0	6.3

[a]Where p_m is the maximum pressure values recorded the during propellant erosion process; Δp is the difference in maximum pressure (p_m) between propellants loaded without and with inhibitors.

https://doi.org/10.1021/acsomega.3c08812
ACS Omega 2024, 9, 9410−9423

(u−p) curves of DB-1# propellants, which can reflect the fact that the burning rate is reduced in the initial burning stage of propellants, indicating that PDMS contact with propellant grain surfaces would affect the burning process of propellants. The burning rate curves of SB#, TB#, DB-2#, and TB# propellants are provided in Figures S21 and S22, which provide support for the same burning rate rules. However, as shown in Figure 16, the p_m of the propellant loading with

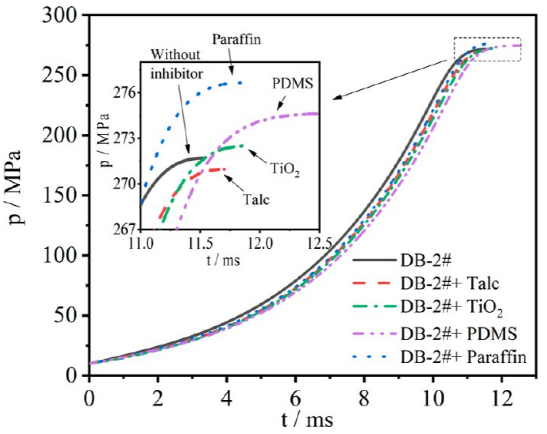

Figure 16. Pressure−time curves of DB-2# propellant loading with the inhibitor in the closed bomb vessel.

PDMS in the closed bomb vessel is higher than the p_m of the propellant charge alone without the inhibitor. This indicated that the decomposition of PDMS also produced a certain volume of gas products in the closed bomb vessel, similar but weaker than paraffin, when the gas venting process was absent.

3.4. Heat Capacity of the Inhibitor by Heat of Explosion Testing. In this work, heat testing of propellant explosions can provide further support in elucidating the variations in erosion-reducing efficiency among different propellants. The heat of explosion (Q) of propellants firing without and with inhibitors was tested using a calorimeter. The percentage change value (Q_P) of heat of explosion for each propellant after additional 3 wt % inhibitors were incorporated, and the inhibitor heat absorption capacity (C/J·g^{-1}) of per gram inhibitor in DB-1# and DB-2# propellant ignition were calculated by the following equations

$$Q_P = [(Q_0 - Q_i)/Q_0] \times 100\%$$

$$C = (Q_0 - Q_i)/0.03$$

where Q_0 (J/g) and Q_i (J/g) were the heat of explosion per gram of propellant ignited without inhibitors and ignited with a 3 wt % inhibitor. Figure 17 shows the results of heat of explosion (Q) and its percentage change values (Q_P) for DB-1# and DB-2# propellants.

According to Figure 17, the Q values of DB-1# and DB-2# propellant were 3285.46 and 5037.23 J/g, respectively. After inhibitor incorporation, the Q values of two propellants were significantly decreased, indicating that the four inhibitors both have heat-absorbing effects on propellant combustion. In the case of DB-1# propellant, as shown in Figure 17a, the Q_P values after talc, TiO_2, PDMS, and paraffin introduction were 0.74, 0.32, 1.12, and 1.08%, respectively. This result suggested that four inhibitors exhibit adjacent Q values in the combustion of propellant with a low flame temperature. While in the case of DB-2# propellant, as shown in Figure 17b, the Q_P values were 0.2, 0.28, 0.75, and 2.82% when talc, TiO_2, PDMS, and paraffin were incorporated, respectively, suggesting the excellent heat-absorption efficiency of paraffin in higher flame temperature propellant combustion compared with the other three inhibitors.

According to the heat capacity (C) calculation of four inhibitors, as shown in Figure 18, it is clearly exhibited that the heat-absorption ability of paraffin increased as propellant flame temperatures enhanced, with C values from 1186.1 to 4737.8 J/g. The tendency can possibly be responsible for the positive erosion-reducing efficiency of paraffin for high flame temperature DB-2# and NB# propellants in the above erosion testing (Figure 2). Moreover, it was also suggested that the effect of cooling propellant gas can be one of the erosion-reduction mechanisms of paraffin at high flame temperatures due to its organic composition, mostly containing $-CH_2$ and $-CH_3$ groups. On the other hand, the heat absorption capacity of PDMS was almost constant in low (2520 K) and high (3677 K) flame temperature combustion, with C values of 1231.6 and 1258.4 J/g, respectively. The main reasons are possibly due to the limited number of $-CH_3$ organic compositions of PDMS having been fully decomposed at low temperature and the fact that the −O−Si−O− groups' inorganic composition of PDMS had relatively low heat absorption ability as the propellant

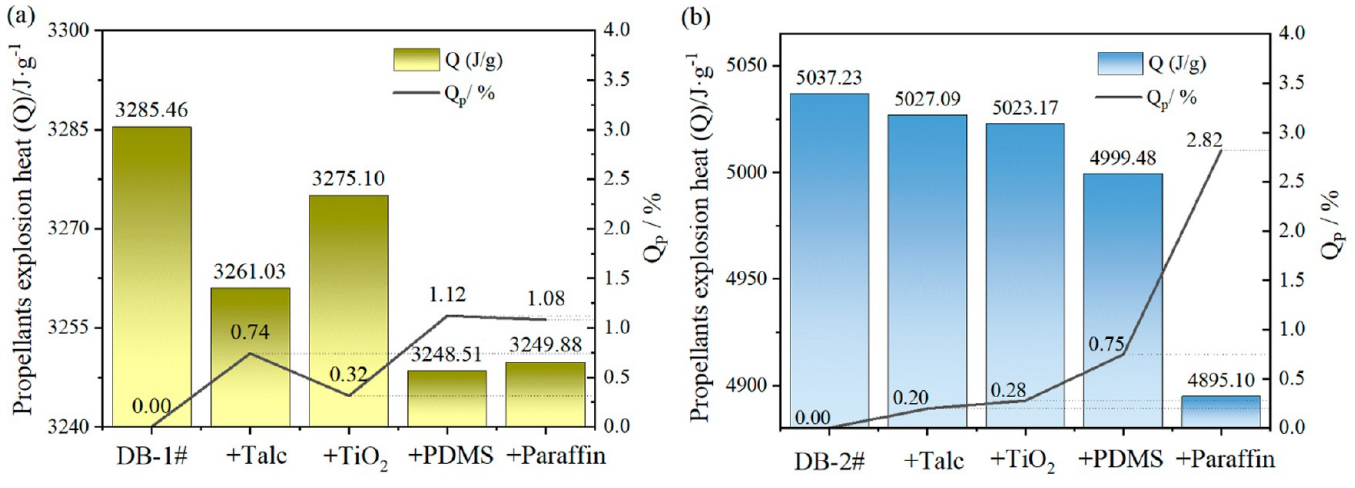

Figure 17. Heat of explosion of (a) DB-1# and (b) DB-2# propellants igniting with inhibitors in a calorimeter.

https://doi.org/10.1021/acsomega.3c08812
ACS Omega 2024, 9, 9410−9423

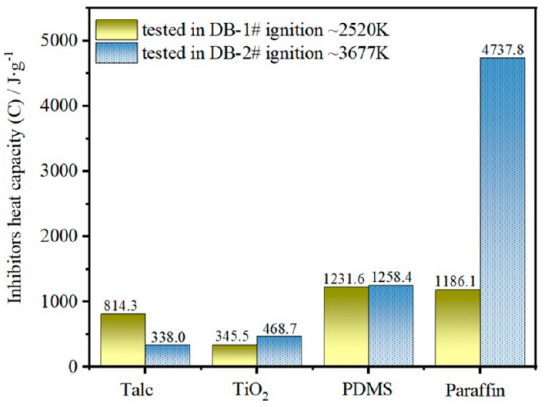

Figure 18. Heat capacity of four representative inhibitors tested by heating effect of propellant burning in a calorimeter.

flame temperature. This resulted in the erosion-reducing efficiency of PDMS is lower than paraffin for DB-2# and NB# propellants with high flame temperatures. Therefore, for high flame temperature propellants, the formation of a silicon oxide particle layer should be the primary erosion-reduced mechanism of PDMS, which is similar to talc and TiO2 inhibitors. While paraffin was supposed to produce a high volume of cool vapor and can mitigate the observed melt-wipe process for the high flame temperature propellant.

3.5. Discussion of the Suitability Matching Relation and Erosion Resistance Mechanisms. Despite some reports preliminarily inferring on the matching relation between inhibitors and propellants composition or gun weapon type,[16,45] systematic research has been rarely conducted in detail so far. Considering the more severe erosion accompanying modern high-energy propellant charges, it is imperative to initiate relevant investigations. However, conducting real artillery firing tests for such studies would require an expensive cost. Hence, exploration using a vented bomb vessel erosion tester becomes necessary.

In this work, according to erosion testing results, talc and TiO_2 particles exhibited a stable positive erosion-reducing effect for DB-1#, SB#, TB#, and DB-2# propellants with theoretical flame temperatures ranging from 2520 to 3677 K. However, the two inhibitors both resulted in more serious erosion for NB# propellants with a flame temperature above 3810 K. There is general consensus in previous studies that particle-like inhibitors, such as Talc and TiO_2, act to mitigate erosion by decreasing heat transfer to the steel interface.[8,20,32] This theory could be supported by the observation results in this work that the particles-like protective layer formed on steel samples when fired by DB-1#, SB#, TB#, and DB-2# propellants. However, as the flame temperature of the NB# propellant increases, the particle inhibitors that are observed to agglomerate contribute to the absence of the protective layer at the steel interface. The phenomenon was related to the structural conversion process of Talc and TiO_2 sintering at high temperature[36−44] that has been discussed in the relevant section above. According to observation results in this work, the erosion occurring process of DB-1# and SB# propellants should derive from the mechanical action of propellant gas flow on the thermally softened steel surface.[6,32] The formation of cracks in steel fired by the TB# propellant derives from stress generated by a steep temperature gradient.[32] Smaller sizes of TiO_2 and talc particle may fill the cracks[32] and lead to a larger area of coverage on the bore surface due to the higher specific surface area and dispersibility of the particles.[19,20] In contrast, the erosion occurring on the steel interface fired by high flame temperatures may have involved a melt-wipe process,[32] which agrees with the erosion observations of DB-2# and NB# propellants in this work. During NB# propellant firing, the aggregated talc and TiO_2 particles with hot gas flow could impact the molten steel interface at high pressure and thereby aggravate the melt-wipe process. Meanwhile, a similar

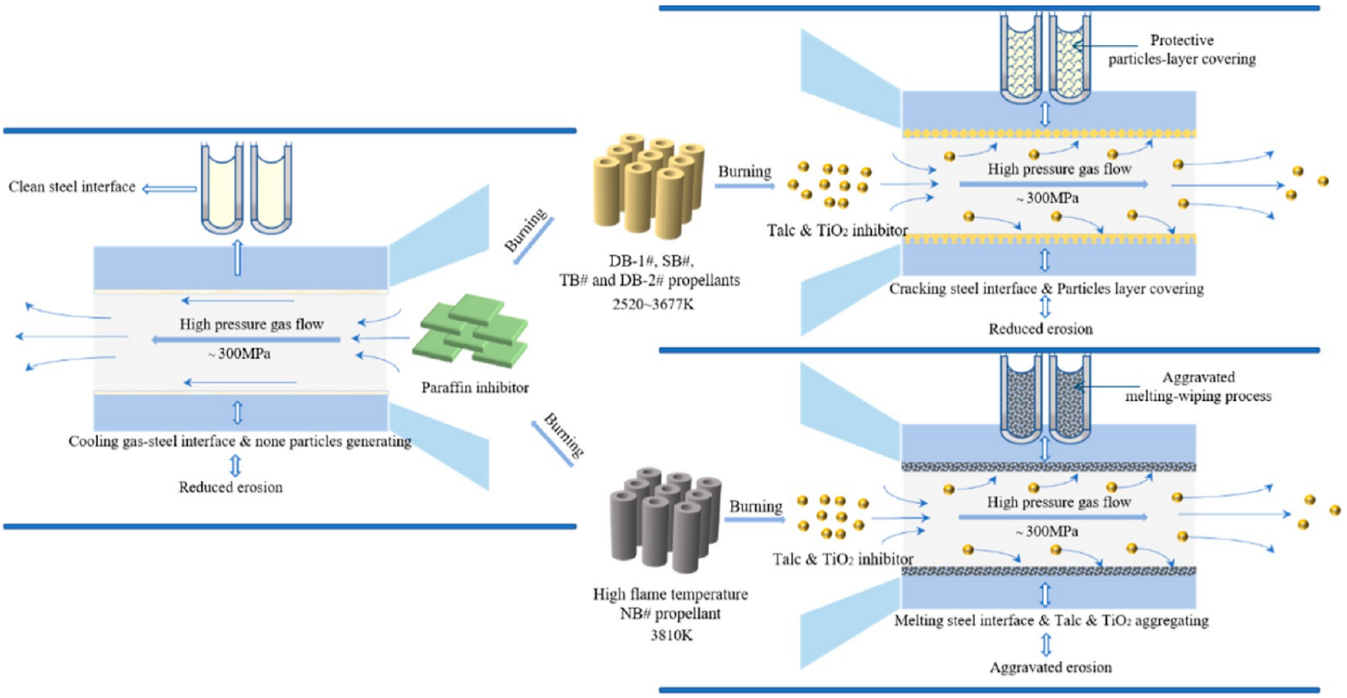

Figure 19. Schematic diagram of the erosion-reducing process and the relevant mechanism.

https://doi.org/10.1021/acsomega.3c08812
ACS Omega 2024, 9, 9410−9423

phenomenon of increased erosion was also reported previously.[20] The particle-like inhibitor, which is not sufficiently dispersed in the propellant matrix, is sintered into large particles during ballistic gun firing, resulting in severe wear on the bore surface. Therefore, the increased flame temperature of the NB# propellant resulting in the same large particles should be the main reason responsible for the invalid erosion-reducing effect for talc and the TiO_2 inhibitor.

On the other hand, the decomposition of PDMS inhibitor at high temperatures also generated numerous particles, which is similar to the decomposition product of talc in chemical structure. It also resulted in a slight increase in erosion for the NB# propellant, but to a lesser extent compared to talc and TiO_2.

In this work, paraffin was the sole material that exhibited unique positive erosion-reducing efficiency for the NB# propellant. This is due to its high heat absorption capacity without particle generation, particularly for the high flame temperature propellant. Meanwhile, the incorporation of paraffin in propellant charges attributed the higher pressure in the bomb vessel tester to this work. From these two aspects, the paraffin can generate a high volume of vapor gas to cool the steel surface and thus mitigate the melt wipe process in NB# propellant firing and significantly reduce its erosion.

Figure 19 schematically sketches out the difference in the erosion resistance process and mechanism of inhibitors in the firing of propellants with quite different flame temperatures. Based on the above analysis, a potential suitability-matching relationship was proposed. Inorganic particle inhibitors and organic paraffin-like inhibitors can both be applied stably to a typical conventional gun propellant with a medium flame temperature due to the protective layer formation of the particle inhibitor and the cooling action of paraffin-like inhibitors. However, for propellants with extremely high flame temperatures, it should be preferred to use inhibitors to generate them without the larger agglomerating particles at high temperatures. This was due to the fact that agglomerated large particles within propellant gas flow could impact the molten steel interface at high pressure and thus possibly aggravate the melt-wipe process. From this perspective, paraffin-like inhibitors with an organic composition having good heat absorption ability and generating high volume gases would be a good alternative, compatibly serving as propellants with high flame temperatures.

3.6. Conclusions. According to erosion testing results, talc, TiO_2, and PDMS exhibited a stable positive erosion-reducing effect for DB-1#, SB#, TB#, and DB-2# propellants with theoretical flame temperatures ranging from 2520 to 3677 K. However, these three inhibitors both resulted in more serious erosion for NB# propellants with a flame temperature above 3810 K. In contrast, paraffin inhibitors exhibited unique positive erosion-reducing efficiency for all propellant samples, particularly including the NB# propellant. Therefore, a potential suitability-matching relationship was proposed. The involved process and mechanism were studied and analyzed through the following aspects:

3.7. Detection of Steel Interface Morphologies and Chemical Compositions Aspects. The erosion occurring in DB-1#, SB#, and TB# propellants with low flame temperatures was primarily the result of the mechanical action of propellant gas flow on the thermally softened steel surface. For the DB-2# and NB# propellants having a higher flame temperature, severe melting was observed at the steel interface.

Subsequently, the morphologies and chemical composition of the steel interface eroded by propellant loading with four inhibitors were detected, respectively. It suggested that the talc, TiO_2, and PDMS inhibitors left particle appearance residues on the steel interface. However, these residue particles exhibited quite different morphologies and structures after different propellant combustions, tending to aggregate into large particles as the propellant flame temperature increased. For the firing of DB-1#, SB#, TB#, and DB-2#, the particles of talc, TiO_2, and PDMS could disperse well on the steel interface and exhibit protective layer features. While firing the NB# propellant at a higher flame temperature, the residues appeared to aggregate into large particles and show increased erosion features. Furthermore, the paraffin loading resulted in an obvious clean steel interface without any particles generating after firing all five propellants. This seemed to be beneficial to mitigate erosion for propellants with a high flame temperature.

3.8. Recording of Propellant Burning Pressure Aspect. According to burning pressure testing in a vented bomb vessel tester, all propellant charges can be regarded as burning and generating erosion in similar pressure conditions of ~300 MPa. The 3 wt % incorporation of Talc, TiO_2 PDMS, and paraffin resulted in the maximum pressure varying by 3.1, 3.3, −3.0, and 6.3 MPa compared to propellants without inhibitor loading. This effect should facilitate the dilution of propellant gases contacting the steel interface.

3.9. Testing of Inhibitor Heat Absorption. Additional 3 wt % inhibitor incorporation led to the heat of explosion of two propellants significantly decreasing, indicating that the four inhibitors both have heat-absorbing effects on propellant combustion. Whereas, paraffin exhibited a higher heat-absorption efficiency as the propellant flame temperature increased compared to the other three inhibitors.

Based on the above analysis in this work, a potential suitability-matching relationship was proposed. Inorganic particle inhibitors and organic paraffin-like inhibitors can both be applied stably to typical conventional gun propellants with low and medium flame temperatures due to the protective layer formation of particle inhibitors and the cooling action of paraffin-like inhibitors. However, for propellants with an extremely high flame temperature, it was suggested to use inhibitors to generate them without the larger agglomerating particles. From this perspective, paraffin-like inhibitors with an organic composition having good heat absorption ability and generating high volume gases would be a good alternative, compatibly serving as propellants with high flame temperatures.

■ ASSOCIATED CONTENT

Supporting Information

The Supporting Information is available free of charge at https://pubs.acs.org/doi/10.1021/acsomega.3c08812.

Experimental parameters, compositions, and properties of propellant samples in this work; schematic diagram of the closed vessel tester and the calorimeter device; erosion-reducing efficiency (E) of propellant loading with inhibitor materials; photograph of steel specimen-fired propellants loaded with Talc, TiO_2, PDMS, and paraffin; EDX chemical element distribution mapping for each erosion tube sample; SEM image of raw talc particles, raw TiO_2 particles, and TiO_2 particles on the steel interface fired by DB-1#/TiO_2 and TB#/TiO_2

https://doi.org/10.1021/acsomega.3c08812
ACS Omega 2024, 9, 9410−9423

propellants; burning time (t_m) of propellants loading with inhibitors in the vented vessel erosion tester; $p-t$ curves of SB#, TB#, DB-2#, and NB# propellants loading with the inhibitor in the vented vessel erosion tester; and $u-p$ curves of SB#, TB#, DB-2#, and NB# propellants loading with inhibitors in a vented vessel erosion tester (PDF)

AUTHOR INFORMATION

Corresponding Authors

Zhitao Liu − *School of Chemistry and Chemical Engineering, Nanjing University of Science and Technology, Nanjing, Jiangsu 210094, China; Key Laboratory of Special Energy Materials, Ministry of Education, Nanjing University of Science and Technology, Nanjing, Jiangsu 210094, China;* orcid.org/0000-0001-6348-0417; Email: liuzhitao331@163.com

Xin Liao − *School of Chemistry and Chemical Engineering, Nanjing University of Science and Technology, Nanjing, Jiangsu 210094, China; Key Laboratory of Special Energy Materials, Ministry of Education, Nanjing University of Science and Technology, Nanjing, Jiangsu 210094, China;* Email: liaoxin331@163.com

Authors

Xijin Wang − *School of Chemistry and Chemical Engineering, Nanjing University of Science and Technology, Nanjing, Jiangsu 210094, China; Key Laboratory of Special Energy Materials, Ministry of Education, Nanjing University of Science and Technology, Nanjing, Jiangsu 210094, China*

Qian Chen − *School of Chemistry and Chemical Engineering, Nanjing University of Science and Technology, Nanjing, Jiangsu 210094, China; Key Laboratory of Special Energy Materials, Ministry of Education, Nanjing University of Science and Technology, Nanjing, Jiangsu 210094, China*

Jing Yang − *School of Chemistry and Chemical Engineering, Nanjing University of Science and Technology, Nanjing, Jiangsu 210094, China; Key Laboratory of Special Energy Materials, Ministry of Education, Nanjing University of Science and Technology, Nanjing, Jiangsu 210094, China*

Yao Zhu − *School of Chemistry and Chemical Engineering, Nanjing University of Science and Technology, Nanjing, Jiangsu 210094, China; Key Laboratory of Special Energy Materials, Ministry of Education, Nanjing University of Science and Technology, Nanjing, Jiangsu 210094, China*

You Fu − *School of Chemistry and Chemical Engineering, Nanjing University of Science and Technology, Nanjing, Jiangsu 210094, China; Key Laboratory of Special Energy Materials, Ministry of Education, Nanjing University of Science and Technology, Nanjing, Jiangsu 210094, China*

Yiming Ma − *School of Chemistry and Chemical Engineering, Nanjing University of Science and Technology, Nanjing, Jiangsu 210094, China; Key Laboratory of Special Energy Materials, Ministry of Education, Nanjing University of Science and Technology, Nanjing, Jiangsu 210094, China*

Feiyun Chen − *School of Chemistry and Chemical Engineering, Nanjing University of Science and Technology, Nanjing, Jiangsu 210094, China; Key Laboratory of Special Energy Materials, Ministry of Education, Nanjing University of Science and Technology, Nanjing, Jiangsu 210094, China*

Complete contact information is available at: https://pubs.acs.org/10.1021/acsomega.3c08812

Notes

The authors declare no competing financial interest.

ACKNOWLEDGMENTS

The authors acknowledge the support of the instrument and equipment fund of the Key Laboratory of Special Energy, Ministry of Education, Nanjing University of Science and Technology.

REFERENCES

(1) Manning, T.; Field, R.; Klingaman, K.; Fair, M.; Bolognini, J.; Crownover, R.; Adam, C. P.; Panchal, V.; Rozumov, E.; Grau, H.; Matter, P.; Beachy, M.; Holt, C.; Sopok, S. Innovative boron nitride-doped propellants. *Def. Technol.* **2016**, *12* (2), 69−80.

(2) Bird, D. T.; Ravindra, N. M. A review: advances and modernization in U.S army gun propellants. *JOM* **2021**, *73*, 1144−1164.

(3) Jaiswal, G.; Shaikh, M. A. R.; Shelar, S. D.; Ramavath, V.; Roy, S. RDX Based Enhanced Energy Propellant for Tank Gun Ammunition. *Propellants, Explos., Pyrotech.* **2020**, *45*, 472−479.

(4) Damse, R. S.; Singh, A.; Singh, H. High energy propellants for advanced gun ammunition based on RDX, GAP and TAGN compositions. *Propellants, Explos., Pyrotech.* **2007**, *32*, 52−60.

(5) Hordijk, A.; Leurs, O. Gun barrel erosion-comparison of conventional and lova gun propellants. *J. Pressure Vessel Technol.* **2006**, *128* (2), 246−250.

(6) Lawton, B. Thermo-chemical erosion in gun barrels. *Wear* **2001**, *251* (1−12), 827−838.

(7) Putti, A.; Chopade, M.; Chaudhari, P. A review on gun barrel erosion. *Int. J. Curr. Eng. Technol.* **2016**, *4*, 231.

(8) Lawton, B. The influence of additives on the temperature, heat transfer, wear, fatigue life, and self ignition characteristics of a 155 mm Gun. *J. Pressure Vessel Technol.* **2003**, *125* (3), 315−320.

(9) Jaramaz, S.; Micković, D.; Elek, P. Determination of gun propellants erosivity: Experimental and theoretical studies. *Exp. Therm. Fluid Sci.* **2010**, *34* (6), 760−765.

(10) Li, X.; Zang, Y.; Mu, L.; Lian, Y.; Qin, Q. Erosion analysis of machine gun barrel and lifespan prediction under typical shooting conditions. *Wear* **2020**, *444*−*445* (15), 203177.

(11) Picard, J. P.; Trask, R. L. A new gun barrel erosion reducer. *J. Spacecr. Rockets* **1968**, *5* (12), 1487−1488.

(12) Richard Ward, J.; Brosseau, T. L. The reduction of barrel erosion by wear-reducing additives. *Wear* **1980**, *60* (1), 149−155.

(13) Fan, W.; Gao, P. A review on erosion-reducing additive materials to extend the lifespan of gun barrels. *J. Mater. Sci.* **2021**, *56*, 19767−19790.

(14) Sun, N.; Xiao, Z. Robust Microencapsulated Silicone Oil with a Hybrid Shell for Reducing Propellant Erosion. *Propellants, Explos., Pyrotech.* **2018**, *43*, 151−155.

(15) Sun, N.; Xiao, Z. Effects of an organic-inorganic nanocomposite additive on the combustion and erosion performance of high energy propellants containing RDX. *Propellants, Explos., Pyrotech.* **2017**, *42*, 1252−1260.

(16) Liang, X.; Ren, Y. Study on Erosion Reduction and useful propellants of inhibitor. *Ordnance Mater. Sci. Eng.* **1997**, *20* (3), 25−30.

(17) Ji, Y.-P.; Zhang, Y.; Lu, X.; Zhou, C. Study on prescription designed of the new type inhibitor. *Chin. J. Explos. Propellants* **2000**, *23* (4), 39−41.

(18) Chen, Y.-c.; Song, Q.; Wang, J. Thermochemical erosion of propellant with nanometer additives. *Acta Armamentarii* **2007**, *28* (3), 329−331.

(19) Song, Q.-z.; Wang, J.; Chen, Y. Research on technology for increasing the service life of gun barrel by adding namomaterial to the propellant. *Trans. Beijing Inst. Technol.* **2007**, *8*, 662−665.

(20) Song, Q.-z.; Wang, J.; Chen, Y.; Duo, Y. Influence of dispersing property of nanomaterial mixed into propellant on the service life of gun barrel. *Acta Armamentarii* **2009**, *30* (3), 289−294.

https://doi.org/10.1021/acsomega.3c08812
ACS Omega 2024, 9, 9410−9423

(21) Yan, J.; Lin, S.; Wang, M.; Zhao, W. Preparation and Characterization of Metatitanic Acid/Urea-Formaldehyde Microcapsules as Wear-Reducing Additives. *Propellants, Explos., Pyrotech.* **2020**, *45*, 1805−1812.
(22) National Military Standard of China. *General specification for double base propellant of gun, GJB 1733A-2009*; National Military Standard of China, 2009 (in Chinese).
(23) National Military Standard of China, *General specification of single base propellant for cannons, GJB 558A-97*; National Military Standard of China, 1997 (in Chinese).
(24) National Military Standard of China, *General specification for triple base propellant, GJB 1529A-2001*; National Military Standard of China, 2001 (in Chinese).
(25) Industry standard of military and civil products. *Gun propellant erosivity test, WJ/Z 259-1990*; Industry standard of military and civil products, 1990 (in Chinese).
(26) Chinese National Standards. *quality carbon structural steels, GB/T 699-1999*; Chinese National Standards, 1999 (in Chinese).
(27) Yang, S. Half closed bomb vessel erosion tube research. *Chin. J. Explos. Propellants* **1986**, *9* (3), 11−16.
(28) Yang, S.; Wang, G. Erosion tube method study. *Chin. J. Explos. Propellants* **1990**, *13* (2), 5−12.
(29) National Military Standard of China. *Test method of propellant, 703.1 method: Closed bomb vessel testing, GJB/770B-2005*; National Military Standard of China, 2005 (in Chinese).
(30) Cote, P. J.; Rickard, C. Gas−metal reaction products in the erosion of chromium-plated gun bores. *Wear* **2000**, *241* (1), 17−25.
(31) Conroy, P.; Nusca, M.; Chabalowski, C.; Anderson, W. *Initial studies of gun tube erosion macroscopic surface kinetics*; Army Research Laboratory, 2001.
(32) Johnston, I. A. *Understanding and predicting gun barrel erosion*; Weapons Systems Division, Defence Science and Technology Organisation (DSTO): South Australia, august, 2005.
(33) Turley, D. M.; Gumming, G.; Gunner, A.; McDermott, I. A metallurgical study of erosive wear in a 105 mm tank gun barrel. *Wear* **1994**, *176* (1), 9−17.
(34) Lavoie, J.; Petre, C.; Dubois, C. Erosivity and performance of nitrogen-rich propellants, Propellants Explos. *Propellants, Explos., Pyrotech.* **2018**, *43*, 879−892.
(35) Perl, M.; Greenberg, Y. Three-dimensional analysis of thermal shock effect on inner semi-elliptical surface cracks in a cylindrical pressure vessel. *Int. J. Fract.* **1999**, *99*, 163−172.
(36) Liu, X.; Liu, X.; Hu, Y. Investigation of the thermal decomposition of talc. *Clays Clay Miner.* **2014**, *62*, 137−144.
(37) Wang, D.; Yi, L.; Huang, B.; Liu, C. High-temperature dehydration of talc: a kinetics study using in situ X-ray powder diffraction. *Phase Transitions* **2015**, *88* (6), 560−566.
(38) Ewell, R. H.; Bunting, E. N.; Geller, R. F. Thermal decomposition of talc. *J. Res. Natl. Bur. Stand.* **1935**, *15* (5), 551−556.
(39) Dellisanti, F.; Valdrè, G. On the high-temperature structural behaviour of talc ($Mg_3Si_4O_{10}(OH)_2$) to 1600°C: Effect of mechanical deformation and strain. *Philos. Mag.* **2010**, *90* (17−18), 2443−2457.
(40) Varghese, O. K.; Gong, D.; Paulose, M.; Grimes, C. A.; Dickey, E. C. Crystallization and high-temperature structural stability of titanium oxide nanotube arrays. *J. Mater. Res.* **2003**, *18*, 156−165.
(41) Balachandran, U.; Eror, N. Raman spectra of titanium dioxide. *J. Solid State Chem.* **1982**, *42* (3), 276−282.
(42) Shi, H.; Zeng, D.; Li, J.; Wang, W. A melting-like process and the local structures during the anatase-to-rutile transition. *Mater. Charact.* **2018**, *146*, 237−242.
(43) Zhang, J.; Li, M.; Feng, Z.; Chen, J.; Li, C. UV Raman spectroscopic study on TiO2. I. Phase Transformation at the surface and in the bulk. *J. Phys. Chem. B* **2006**, *110* (2), 927−935.
(44) Leth-Miller, R.; Jensen, A. D.; Glarborg, P.; Jensen, L.; Hansen, P.; Jørgensen, S. Experimental investigation and modelling of heat capacity, heat of fusion and melting interval of rocks. *Thermochim. Acta* **2003**, *406*, 129−142.
(45) Zhang, X. *Interior Ballistics of Guns*; Beijing Institute of Technology Press: Beijing, 2014, pp 206−210.

https://doi.org/10.1021/acsomega.3c08812
ACS Omega 2024, 9, 9410−9423